

# When Cars meet Drones: Hyperbolic Federated Learning for Source-Free Domain Adaptation in Adverse Weather

Giulia Rizzoli\*<sup>①</sup>, Matteo Caligiuri\*<sup>①</sup>, Donald Shenaj<sup>①</sup>, Francesco Barbato<sup>①</sup>,  
and Pietro Zanuttigh <sup>①</sup>

University of Padova, Italy  
firstname.lastname@dei.unipd.it

**Abstract.** In Federated Learning (FL), multiple clients collaboratively train a global model without sharing private data. In semantic segmentation, the Federated source Free Domain Adaptation (FFREEDA) setting is of particular interest, where clients undergo unsupervised training after supervised pretraining at the server side. While few recent works address FL for autonomous vehicles, intrinsic real-world challenges such as the presence of adverse weather conditions and the existence of different autonomous agents are still unexplored. To bridge this gap, we address both problems and introduce a new federated semantic segmentation setting where both car and drone clients co-exist and collaborate. Specifically, we propose a novel approach for this setting which exploits a batch-norm weather-aware strategy to dynamically adapt the model to the different weather conditions, while hyperbolic space prototypes are used to align the heterogeneous client representations. Finally, we introduce FLYAWARE, the first semantic segmentation dataset with adverse weather data for aerial vehicles.

## 1 Introduction

The field of autonomous driving has evolved significantly beyond the traditional concept of cars navigating city streets. In the contemporary landscape, autonomous navigation encompasses various perspectives, including drones and robots, serving a wide range of applications like autonomous delivery and surveillance. The demand for intelligent systems that can seamlessly generalize across these varying viewpoints is quickly increasing, to enhance safety, efficiency, and adaptability. A key challenge lies in achieving this goal while preserving confidentiality and data security. The importance of robust privacy measures in developing autonomous systems cannot be overstated, as these systems often rely on substantial amounts of data to function effectively. The traditional method of gathering and analyzing data in a centralized manner raises relevant security concerns. Federated learning allows tackling this issue by introducing a cutting-edge paradigm that enables the collaborative training of machine learning models

---

\* These authors contributed equally to this work.

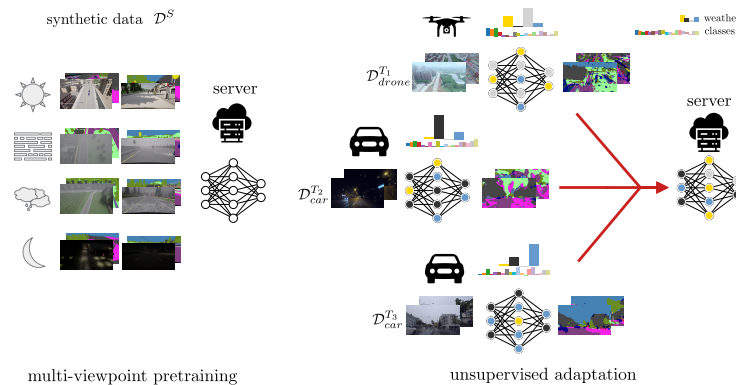


**Fig. 1:** Overview of the considered setting: after a supervised pretraining on synthetic data, a heterogeneous set of unsupervised clients collaboratively optimize their model in a federated fashion. Notably, adapting the model also to varying weather conditions.

without sharing the private data of the participants (*i.e.*, clients). In this paper, we introduce a novel federated learning approach tailored to the specific challenges encountered in driving scenarios, where autonomous agents have different viewpoints, specifically the street-view vision for cars and the aerial for UAVs. Multi-viewpoint paradigms have been proven beneficial in various tasks among which localization and segmentation [18,31,35], where jointly training the model with images from different viewpoints improves the objective task. Consequently, we enhance our framework by integrating aerial data. Moreover, we exploit this strategy in combination with the recent federated learning paradigm proposed in [37] that exploits a supervised server pretraining to enable unsupervised training on the client side. Additionally, our approach not only enables knowledge sharing between clients with different identities - either cars or drones - but also dynamically adapts to ever-changing weather conditions, aligning with the real-world challenges in this dynamic field. In this scenario (shown in Fig. 1), several key challenges arise:

1. Clients operating without supervision tend to become overly confident in their predictions, causing the model to diverge.
2. Clients exhibit differing distributions, and varying weather conditions can significantly impact performance (*i.e.*, clients are non-iid, *heterogeneous*).
3. Clients are unbalanced, reflecting real-world scenarios where certain types of agents may be less common (*e.g.*, fewer drones compared to cars).

To address these challenges, we present several novel contributions:

- We introduced an unsupervised federated learning system for autonomous cars that can benefit from aerial view integration and seamlessly switch between the two perspectives.

- We introduced HyperFLAW (Hyperbolic Federated Learning in Adverse Weather), which addresses domain shifts in diverse weather conditions using weather-aware batch normalization layers and integrates the first semantic segmentation dataset with adverse weather imagery for aerial vehicles.
- We exploited prototype-based learning in the hyperbolic space to ensure consistent training across the clients in this very challenging setting.

## 2 Related Work

**Domain Adaptation** (DA) primarily focuses on adapting a model from a source to a target domain, typically in scenarios where the target data lacks labels, referred to as Unsupervised Domain Adaptation (UDA) [36, 43]. Historically, DA methods aimed to bridge the gap by quantifying domain divergence [33, 45]. Adversarial learning has also been widely used [24, 30, 44]. In the contemporary landscape, advanced approaches [15, 28, 54] leverage self-learning techniques. Several other approaches have been used to align the domains such as image-to-image translation [1, 6, 47], pseudo-label prototypes [23, 50, 51], and confidence thresholding [28, 54]. Within the objective of adapting to adverse weather conditions, Bruggemann et al. [3] propose a solution that requires sunny daytime references. To tackle nighttime images, Xiao et al. [46] employed a data augmentation method leveraging multiple modalities. Finally, Source Free Domain Adaptation (SFDA) presents a distinct advantage in addressing the performance gap by allowing adaptation without access to labeled source data [19].

**Federated Learning** has captured the interest of the research community due to its practical applicability in various real-world scenarios and its potential to manage sensitive data [27]. In literature, it has been applied to different vision tasks [38], initially with a large emphasis on classification [20, 21], but more recently also focusing on other tasks including semantic segmentation for Autonomous Driving [5, 11, 37]. Most existing works in FL assume labeled data on remote clients [5], which is an unrealistic assumption, especially in the driving scenario. Notably, Shenaj et al. [37] introduce the Federated source Free Domain Adaptation (FFREEDA) setting, where only the server accesses a labeled source dataset. We address this challenge by incorporating the management of diverse viewpoints, accommodating various client types, and dealing with the influence of adverse weather conditions.

**Hyperbolic Prototypical Learning.** Working in Euclidean spaces, implicitly or explicitly assume that data is best represented on regular grids. While this model offers an intuitive and grounded underlying manifold, its properties may not be the most suitable for all types of data [29]. Inspired by developments in other fields, deep learning in hyperbolic space has recently been exploited in computer vision using different isomorphic models, such as the Poincaré model. Several works have proposed prototypes-based hyperbolic embeddings for few-shot learning for classification [14, 17, 26], where hyperbolic space offers advantages over the Euclidean one. In particular, Khrulkov et al. [17] demonstrated its competitiveness on simple ConvNets while Gao et al. [12] show the benefits

achievable with different curvatures. Atigh et al. [2] introduced approximations for faster computations tailored for use in semantic segmentation. Facing these insights, hyperbolic prototypical learning seems suitable for learning features robust to domain shift and varying weather conditions even when employing different curvatures and lightweight networks, as those used on clients in federated scenarios. Building upon these foundations, our approach exploits hyperbolic learning to align features from diverse viewpoints while reducing domain shift.

### 3 Problem Formulation

Most works in Federated Learning operate under the assumption of labeled data being available on remote clients [5]. Providing semantic segmentation ground truth is extremely time-consuming and costly, thus it is quite unrealistic to expect labeled data on real-world clients, especially during the deployment phase. Therefore, our objective is to develop a model that can seamlessly adapt from labeled synthetic data to unlabeled real-world images in a distributed paradigm. For this reason, we chose to deploy our setting on top of the pre-existing FFREEDA scenario [37]. Moreover, we discard the assumption that the clients are homogeneous in nature and consider a setting where different autonomous agents work cooperatively in fluctuating atmospheric conditions (*i.e.*, clear sky, night, rain and fog). In the following, we will first formalize the problem and then move to a detailed description of the methodologies proposed to tackle it in Sec. 4.

**Source-Free Domain Adaptation (SFDA).** Consider an image  $x \in \mathcal{X} \subset \mathbf{R}^{|\mathcal{I}| \times 3}$  and its corresponding label  $y \in \mathcal{Y} \subset \mathbf{R}^C$ , where  $|\mathcal{I}| = H \times W$  are the image dimensions and  $C$  is the number of classes. SFDA entails a pretraining phase on a source dataset  $\mathcal{D}^S = \{(x^s, y^s)\}^{N^S}$ , made of pairs of images and labels, and an adaptation stage on a target dataset  $\mathcal{D}^T = \{(x^T)\}^{N^T}$ , composed of unlabeled images. Specifically, compared to standard DA: 1) the two training phases are distinct; 2)  $\mathcal{D}^S$  is unavailable at the adaptation phase.

**Federated source-Free Domain Adaptation (FFREEDA).** This setting deals with a distributed setup comprising a central server and a set of clients  $\mathcal{K}$  with  $|\mathcal{K}| = K$ . The training datasets are organized as follows: the primary dataset  $\mathcal{D}^S$ , resides on the server side. Concurrently, each of the  $K$  client has a distinct training dataset denoted as  $\mathcal{D}_k^T = \{x_{k,i}^T \in \mathcal{X} : \forall i \in |\mathcal{D}_k^T|\}$ . Notably, these client datasets are locally stored and managed, ensuring that  $\mathcal{D}_1^T \cap \mathcal{D}_2^T \cap \dots \cap \mathcal{D}_K^T = \emptyset$ . In distributed settings, the parameter  $K$  is reasonably large, and the local datasets vary in terms of statistics, *i.e.* size and distribution. However, they typically possess a much smaller size compared to the source dataset ( $N^S \gg N^T$ ). FFREEDA assumes that the local datasets are drawn from the same meta-distribution, meaning that  $\mathcal{D}_k^T$  comprises images solely from one latent domain. The objective is to achieve optimal segmentation performance on the target data distribution with the model  $M(\theta) : \mathcal{X} \rightarrow \mathbf{R}^{|\mathcal{I}| \times |\mathcal{Y}|}$ , parameterized by  $\theta$ . This goal

is pursued by minimizing an appropriate loss function, expressed as:

$$\theta^* = \arg \min_{\theta} \sum_{k \in [K]} \frac{|\mathcal{D}_k^T|}{|\mathcal{D}^T|} \mathcal{L}_k(\theta) \quad (1)$$

where  $\mathcal{L}_k$  represents the local loss function, and  $\mathcal{D}^T = \bigcup_{k \in \mathcal{K}} \mathcal{D}_k^T$ .

**Multi-viewpoint FFREEDA in Adverse Weather.** Aiming to assist agents lacking large training datasets or capabilities, such as drones, we consider a setting that enables scene understanding for unsupervised autonomous navigation robust to multiple viewpoints. First of all, we consider  $\mathcal{D}^S = \mathcal{D}_{car}^S \cup \mathcal{D}_{drone}^S$ . Accounting for adverse weather as a heterogeneity factor, our dataset  $\mathcal{D}^S = \{(\mathbf{x}^S, \mathbf{y}^S, w^S)\}^{N^S}$  also includes  $w^S$ , denoting the atmospheric condition for each frame, together with the color images  $\mathbf{x}^S$  and the ground truth segmentation maps  $\mathbf{y}^S$ . Similarly, the client can accommodate either car or drone agents:  $\mathcal{D}^T = \mathcal{D}_{car}^T \cup \mathcal{D}_{drone}^T$ , although clients datasets are still local and disjoint. As in the previous setting, each client  $k \in \mathcal{K}$  have its own set of unsupervised images both in terms of semantics and weather:  $\mathcal{D}_k^T = \{(\mathbf{x}_k^T)\}$ . Notably, the number of samples of the drones’ target dataset ( $N_{drone}^T$ ) is typically lower than in the target datasets for cars ( $N_{car}^T$ ). Furthermore, the set of semantic classes could differ between car and aerial vehicles datasets (in our case  $C_{drone} \subset C_{car} = C^T = C^S$ ). The identity of each client is fixed, meaning it is designated as either a car or a drone and does not change during training, however, there is no such limitation on the weather conditions, which can change dynamically during the training process. The goal is to minimize the objective function of Eq. (1), where the target data distribution holds into its heterogeneity different viewpoints and weathers. In Fig. 2 we present our approach, which will be detailed in Sec. 4.

## 4 Training Procedure

The training is organized in a set of rounds  $r = 0, \dots, R$ , where  $r = 0$  corresponds to the pretraining phase. At each round  $r$ , we denote by  $M_G^r$  the global model at the server side, while we refer to  $M_k^r$  as the model of the  $k$ -th client.

**Pretraining.** We train the initial model  $M_G^0$  on a large-scale source synthetic dataset  $\mathcal{D}^S$ , taking advantage of the server’s computing capabilities. By sampling batches of cross-agent we maximize the standard cross entropy loss  $\mathcal{L}(y^S, M_G^0(x^S))$ .

Moreover, an additional component  $M_W$  consisting of 3 convolutional layers is trained to recognize weather conditions by optimizing  $\mathcal{L}(w^S, M_W(x^S))$ . This classifier is a lightweight module intended to provide weather information for clients and it is not trained after this phase. Differently from [37], we do not assume to have information on the clients’ distribution (i.e., in [37] the average Fourier domain coefficients from  $\mathcal{D}^T$  are used, requiring priors on clients’ data).

**Adaptation.** At each round  $r$ , we consider that, among all the set of clients  $\mathcal{K}$ , only a subset denoted as  $\mathcal{K}^r$  participate in the training. This assumption is common in FL where not all the clients might be concurrently active and reflects

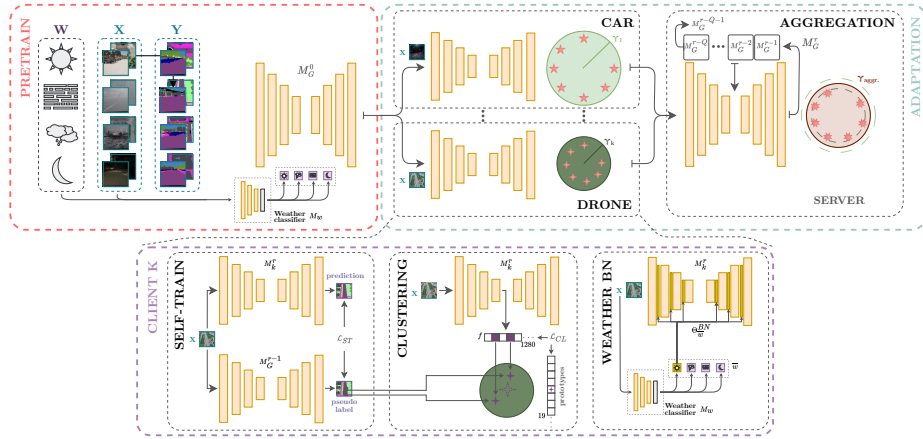


**Fig. 2:** The two-step training process of HyperFLAW: server pretraining on synthetic data and client-side real-world adaptation. We highlight the active modeling of weather conditions using weather-aware batch norm layers and the use of hyperbolic space for feature alignment via prototypical learning, ensuring consistency in features extracted by car and drone agents across various atmospheric conditions. At the server, the aggregation with the queue of previous global models reduces the instability introduced by aggregating unlabeled clients.

well on our scenario (e.g. a car is parked). Then, the server transmits the global model from the previous round  $M_G^{r-1}$ . Note that the weather classifier  $M_W$  is only transmitted once as it is fixed. The training for the active clients will be performed separately on  $M_k^r, k \in \mathcal{K}^r$ . Furthermore, a prototype representation  $\mathbf{p}_{c,k}^r$  for each class (i.e., the centroids of the class samples in feature space) is also built and transmitted to the server together with the manifold curvature  $\gamma_k$  (refer to Sec. 4.3). Finally, the models are aggregated at the server side with the approach of Sec. 4.4 obtaining the global model  $M_G^r$  that is used as input for the next step. Prototypical representations are also aggregated at the server side obtaining a set of global class prototypes  $\mathbf{p}_{G,c}^r$ .

#### 4.1 Client Self-Training (ST)

Self-training involves iteratively enhancing a model’s performance by using its own predictions. In FL, the clients can rely on the server model as the teacher, as ideally, the server aggregates the global knowledge from the targets. In our framework, we update the teacher model after the round is over. This implies that the global model received by the clients at the beginning of each round  $r$ ,  $M_G^{r-1}$ , serves also as the current teacher. This approach offers the advantage of eliminating the necessity to transmit two models per round as in [37] where also a model from  $R_u$  steps before was used, thus requiring only a single model transmission and avoiding the extra hyperparameter  $R_u$ . The local model of the  $k$ -th client is trained using the weak supervision of the pseudo-labels produced

by the teacher model  $M_G^{r-1}$  and its local model prediction  $M_k^r$  by optimizing the self-training loss obtained via cross-entropy as  $\mathcal{L}_{st}(M_G^{r-1}(x_k^T), M_k^r(x_k^T))$ . Moreover, to achieve a training that is consistent across the heterogeneous clients and a model able to generalize to different types of agents and weather conditions the self-training loss is used in combination with the prototype-based one, i.e.,

$$\mathcal{L}_k(\theta) = \mathcal{L}_{st}(\theta) + \lambda_{cl}\mathcal{L}_{cl}(\theta) \quad (2)$$

where  $\theta$  are the model parameters,  $\mathcal{L}_{cl}$  is the clustering loss computed using prototypical representation (see Sec. 4.3), and  $\lambda_{cl}$  balances the two losses.

## 4.2 Weather Batch Normalization (BN)

Inspired by [22] where the update of the batch normalization layers is not synchronized within the global model, we personalize the training by considering a different set of batch-normalization (BN) parameters for each weather condition  $w$ , defined as  $\{\theta_w^{BN}\}$ . After the pretraining ( $r = 0$ ), all the weather-specific BNs inherit the global BN statistics  $\theta^{BN}$ , while in each subsequent round, the statistics of the BNs are averaged only over those of the same weather condition. Specifically, on the client side, after obtaining the prediction  $\bar{w} = M_W(x^T)$  from the classifier, the client batch-norm parameters are optimized using Eq. 2 only on the selected weather-BNs  $\theta_{\bar{w}}^{BN}$ . This allows us to enforce a more general feature extraction from the convolutional layers while exploiting the domain-specific nuances of road scenes under different weather conditions.

## 4.3 Prototypical Learning

While the various devices explore road scenes, their distinct viewpoints force the local models to conform more closely to the features within each specific perspective. In the pretraining phase, drone and car samples are provided jointly, however, this simultaneity does not apply to clients, thereby the network predictions could diverge, making the subsequent aggregation on the server side more challenging. To ensure the ongoing alignment of features across the two data types, we propose the exploitation of joint class prototypes as a viable solution. For each client, we compute a set of class prototypes  $\mathcal{P}$ , where each prototype  $\mathbf{p}_c \in \mathcal{P}$  is defined as a function of the set  $\mathcal{F}_c$  of all feature vectors  $\mathbf{f}_c$  from the encoder output that are associated to class  $c$ :

$$\mathbf{p}_c = g(\mathcal{F}_c), \mathcal{F}_c = \{\mathbf{f} = E(\mathbf{x})(h, w) : \hat{\mathbf{y}}(h, w) = c\} \quad (3)$$

where  $\hat{\mathbf{y}}$  are the teacher pseudo-labels subsampled at the feature space resolution and the function  $g$  computes either the mean or the midpoint depending on the considered manifold: Euclidean or Poincaré Ball, respectively.

At the beginning of each round  $r$ , a participating client  $k$  initializes its local prototypes  $\mathbf{p}_{\mathbf{k},c}^r$  using the previous round ones received from the server:  $\mathbf{p}_{\mathbf{k},c}^r =$

$\mathbf{p}_{G,c}^{r-1}$ . Then, the prototypes are updated at training time using exponential smoothing with rate  $\beta = 0.85$  to stabilize their evolution as follows:

$$\mathbf{p}_c = \beta \mathbf{p}'_c + (1 - \beta) \mathbf{p}_c \quad (4)$$

where  $\mathbf{p}'_c$  is the prototype from the previous step. After each round, prototypes  $\mathbf{p}'_{k,c}$ ,  $\forall c \in \mathcal{C}$  computed by each client are sent back to the server for aggregation. **Hyperbolic Protoypes.** As mentioned before, to further improve performance, we exploited the capacity of hyperbolic space - specifically of the Poincaré ball model - to fit complex feature geometries better and used it to embed the prototypes. We refer to [29,40] for further discussion. The hyperbolic space represented in Riemannian geometry, with dimension  $n$  and constant negative curvature  $-\gamma$  is expressed as:

$$\mathbb{B}_\gamma^n = \{\mathbf{x} \in \mathbb{R}^n : \|\mathbf{x}\|^2 < 1/\gamma\} \quad (5)$$

On such space, the distance between two points  $\mathbf{x}, \mathbf{y} \in \mathbb{B}_\gamma^n$  can be computed as:

$$d_\gamma(\mathbf{x}, \mathbf{y}) = \left( \frac{2}{\sqrt{\gamma}} \right) \tanh^{-1}(\sqrt{\gamma} \|\mathbf{x} \oplus_\gamma \mathbf{y}\|) \quad (6)$$

where  $\mathbf{x} \oplus_\gamma \mathbf{y}$  is the Möbius addition:

$$\mathbf{x} \oplus_\gamma \mathbf{y} = \frac{(1 + 2\gamma\langle \mathbf{x}, \mathbf{y} \rangle + \gamma\|\mathbf{y}\|^2)\mathbf{x} + (1 - \gamma\|\mathbf{x}\|^2)\mathbf{y}}{1 + 2\gamma\langle \mathbf{x}, \mathbf{y} \rangle + \gamma^2\|\mathbf{x}\|^2\|\mathbf{y}\|^2} \quad (7)$$

The translation from the Euclidean to the hyperbolic space is obtained given the exponential mapping in the direction of a tangent vector  $\mathbf{v} \in \mathcal{T}\mathbb{B}_\gamma^n$ :

$$\exp_\gamma(\mathbf{v}) = \mathbf{x} \oplus_\gamma \left( \tanh \left( \frac{\sqrt{\gamma}\|\mathbf{v}\|}{1 - \gamma\|\mathbf{v}\|^2} \right) \frac{\mathbf{v}}{\sqrt{\gamma}\|\mathbf{v}\|} \right) \quad (8)$$

The prototypes are determined as the midpoints of the hyperbolic feature vectors  $\{\mathbf{f}_i := \mathbf{f}_i^{hyp} \in \mathbb{B}_c^n\}$ , using an approximation of the Frechet mean:

$$\mathbf{p} = \frac{1}{2} \otimes_\gamma \frac{\sum_{\mathbf{f} \in \mathcal{F}} \lambda_{\mathbf{f}}^\gamma \mathbf{f}}{\sum_{\mathbf{f} \in \mathcal{F}} (\lambda_{\mathbf{f}}^\gamma - 1)} \quad (9)$$

where the Möbius scalar multiplication is:

$$r \otimes_\gamma \mathbf{x} = \frac{1}{\sqrt{\gamma}} \tanh(r \tanh^{-1}(\sqrt{\gamma}\|\mathbf{x}\|)) \frac{\mathbf{x}}{\|\mathbf{x}\|} \quad (10)$$

Since the curvature  $\gamma$  is a scalar value, we can convert it to a learnable parameter of the network and optimize it during the training process [41]. This is done on the client side using self-supervision and prototype loss, then, at the end of each round, the curvature of the active clients is aggregated using *FedAvg* algorithm, i.e., the average is weighted by the number of seen samples.

**Prototypical Loss.** Due to the distribution mismatch between source and target domains and the different viewpoints, feature vectors from these domains



become misaligned, leading to inaccuracies in target representations and a subsequent decline in segmentation accuracy. To address this issue, we adopt a clustering objective in the latent space by leveraging prototypical representations:

$$\mathcal{L}_{cl} = \frac{1}{|\hat{\mathcal{C}}|} \sum_{c \in \hat{\mathcal{C}}} \frac{1}{|\mathcal{F}_c|} \sum_{\mathbf{f}_c \in \mathcal{F}_c} d(\mathbf{f}_c, \mathbf{p}_c) \quad (11)$$

where  $\hat{\mathcal{C}} := \{c \in \mathcal{C} : |\mathcal{F}_c| > 0\}$  is the set of active classes in the current batch.

#### 4.4 Server Aggregation (AG)

**Regularization.** As mentioned earlier, the wide range of data variability across client devices, caused by various types of autonomous agents and changing weather conditions, makes aggregation at the server side challenging. Moreover, unrestricted self-training on the client side can lead to instability (see training curve when only  $\mathcal{L}_{st}$  is active in Fig. 4) and to a decrease in performance after several rounds. To stabilize the results with respect to standard averaging [27], we used a combination of the models received from the clients with the global ones available at server side from previous steps. In this way, during the first rounds, there is a smoother adaptation from the pretrained model. More in detail, the aggregated model on the server side is computed as:

$$M_G^r = \frac{\sum_{k \in \mathcal{K}^R} M_k^r}{|\mathcal{K}^R|} + \sum_{j=1}^Q M_G^{r-j} \quad (12)$$

i.e., we get the output of federated averaging and smooth it by averaging with the  $Q$  previous rounds, thus making the learning more stable [4, 39]. Other approaches [37] tackle regularization by exploiting the global model from several snapshots ago, *i.e.*  $M_G^0$ . The idea behind this is to distill knowledge from past predictions, where the server has higher confidence. However, this introduces additional transmission requirements at each round or necessitates clients to allocate resources for storing  $M_G^0$ . Moreover, clients must perform additional inference and computation for each image. We address these challenges by implementing a strategy that only requires effort from the server side, *i.e.*, by maintaining a queue of previous model snapshots ( $Q$ ). We ensure that the burden falls on the server, where memory and computational capabilities are less constrained. We will denote this aggregation strategy as AG in the results to distinguish it from standard FedAvg.

**Prototype aggregation.** Prototypes are also aggregated on the server side. To this aim, we used a combination of the previously computed prototypes and the ones received by the clients. To determine the updates, we calculated a weighted average of the prototypes received by the clients and smoothed the result by considering the prototypes from the previous round:

$$\mathbf{p}_{G,c}^{r+1} = \beta' \mathbf{p}_{G,c}^{r-1} + (1 - \beta') \sum_{k \in \mathcal{K}^r} N_{k,c}^r \mathbf{p}_{k,c}^r \quad (13)$$

where  $N_{k,c}^r = |\mathcal{F}_{k,c}|$  at round  $r$  and  $N_c^{r,tot} = \sum_{k \in \mathcal{K}} N_{k,c}$ . We used the same smoothing parameter of Eq. (4), i.e.,  $\beta^t = \beta = 0.85$ .

**Table 1:** Data distribution (†: with Cityscapes as clear, see Suppl. Mat. )

			Clear	Night	Rain	Fog
SYNTH	SELMA	Train	24735	24735	24735	24735
		Test	3087	3087	3087	3087
	FLYAWARE-S	Train	24771	24731	24808	24631
		Test	3147	3139	3128	2935
ACDC†	Train	1060	400	400	400	
	Test	214	100	100	100	
REAL	FLYAWARE-R	Train	94	35	35	35
		Test	18	18	17	17
	FLYAWARE-R-XL	Train	565	565	565	565
		Test	112	53	52	52

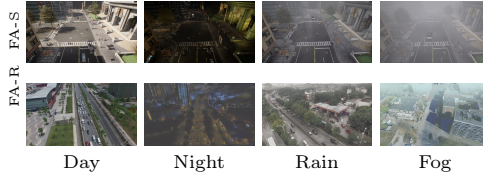


**Fig. 3:** Samples from different datasets under varying weather conditions.

## 5 The FLYAWARE Adverse Dataset

In standard autonomous driving for semantic segmentation, there is a sufficient number of datasets providing a diversity of adverse conditions [34, 42]. However, in the case of aerial viewpoints, a scarcity of such datasets is evident, thus making the development of a dataset of this type a priority to unlock further research on the topic. To this aim, we introduce a new benchmark FLYAWARE - FLYing in Adverse Weather: Artificial and REal data. In the following section, we outline the structure of the synthetic and real aerial datasets,  $\mathcal{D}_{drone}^S$  and  $\mathcal{D}_{drone}^T$ , respectively. They contain over 100K for which we contribute with 108180 generated images and 1287 domain-translated ones. In Tab. 1, we present the datasets used in this study. For additional information regarding the datasets for autonomous cars, please consult the Suppl. Mat.

**FLYAWARE-S: Adverse Synthetic Dataset.** Recently released, Syn-drone [32] is a synthetic dataset based on the CARLA simulator [8]. While the dataset is richly annotated with 28 semantic classes, it currently lacks imagery in different weather conditions. We extended their work starting from the code-base provided in [32] by generating images in 3 adverse weather conditions (*i.e.*, rain, fog, and night), while maintaining the capability of the system to produce images from multiple viewpoints and heights. The dataset includes drone views at heights ranging from 20 to 80 meters and with angles varying from 30 to 90 degrees, all with a resolution of 1920x1080. Moreover, we also generated 3D data (depth maps and LiDAR) for future usage in multimodal architectures.

**FLYAWARE-R: Real Dataset Translation.** Since no adverse weather dataset for aerial vehicles is available we opted for using image translation over standard drone datasets to build the adverse weather imagery. Addressing the

task of converting daytime images into adverse conditions requires the availability of images of clear weather samples like sunny or cloudy conditions, and of adverse samples occurring in specific conditions of interest, such as rainy weather. Inspired by [13] which performs adverse domain translations for autonomous driving in the context of depth estimation, we opted for the use of Generative Adversarial Networks (GANs). For the rain and night adverse conditions, we employed the ForkGAN model [52] to translate clear-day training samples from the UAVid dataset [25]. While for the fog samples, we have used a combination of Omnidata [10] and FoHIS [49] methods. In the following, we will present an in-depth explanation of how we have performed the aforementioned conversion.

**Day2Night.** To convert daylight into nighttime, we trained ForkGAN over 14K images, half of which represent daytime and the other half nighttime. All the used images were sampled from Visdrone [53], and UAVDT [9], two datasets designed for Object Detection. We have decided to sample the training data from different datasets to increase the overall number of nighttime images. This was necessary to ensure that the GAN architecture reaches good enough reconstruction performance. The training phase lasted 40 epochs. After the training, for all the nighttime samples in the UAVid dataset, we convert clear-day images into their nighttime counterparts using the pretrained model.

**Day2Rain.** Training the GAN models directly on drone data proved advantageous as it helped to mitigate domain shifts. In the rain case however there are no available drone datasets - not even for other tasks as in the case of night images -, therefore we had to train ForkGAN using diverse datasets that included adverse weather scenarios, like BDD100K [48], ACDC [34] and RainCityscapes [16] (which are datasets for automotive applications). For daytime to rainy conversion, we followed the same strategy applied for the conversion to nighttime training the ForkGAN model over 9K images for 40 epochs and we applied the pretrained model to convert images into their rainy counterparts.

**Day2Fog.** To perform daytime to foggy conversion we first estimated a depth map for each image in the UAVid dataset using Omnidata [10], then, we exploited the estimated depth as input to the FoHIS method [49] to apply fog.

**Federated Splits.** We consider two scenarios: the first is an unbalanced setup with 40 clients, corresponding to 32 automotive clients and 8 drones; the second is more balanced having 32 automotive clients and 32 drones, however the training and test set of the drones come from two different domains. Aligned with previous works [37], the clients have a different number of samples associated with them, in particular, the number of samples in each client is in the range [69, 72] for cars and [24, 25] for drones. To simulate real scenarios, we assumed that the most common weather would be clear daytime, while clients can have different combinations of adverse weather. Refer to the Suppl. Mat. for the weather distribution details on clients.

**Table 2:** mIoU on the target datasets (ACDC and FLYAWARE-R (FA-R)).

Setting	Train	Test	Method	Car	Drone	All
centralized	FA-S+SELMA	ACDC+FA-R	Source Only	19.96	33.11	22.70
centralized	ACDC+FA-R	ACDC+FA-R	Target Only	60.17	50.14	58.08
federated	ACDC+FA-R	ACDC+FA-R	Fine-Tuning	34.35	39.10	35.34
FFREEDA	ACDC+FA-R	ACDC+FA-R	FedAvg [27]+ST	25.00	30.25	26.10
FFREEDA	ACDC+FA-R	ACDC+FA-R	LADD [37]	25.95	30.79	26.96
FFREEDA	ACDC+FA-R	ACDC+FA-R	<b>HyperFLAW</b>	<b>27.45</b>	<b>34.69</b>	<b>28.96</b>
centralized	FA-S+SELMA	ACDC+FA-R-XL	Source Only	19.96	32.61	22.61
FFREEDA	ACDC+VisDrone	ACDC+FA-R-XL	FedAvg [27]+ST	22.76	31.55	24.59
FFREEDA	ACDC+VisDrone	ACDC+FA-R-XL	LADD [37]	26.32	28.93	26.86
FFREEDA	ACDC+VisDrone	ACDC+FA-R-XL	<b>HyperFLAW</b>	<b>27.10</b>	<b>35.45</b>	<b>28.84</b>

## 6 Implementation Details

**Datasets.** In this study, we leveraged two synthetic driving datasets - one collected from cars and one from drones - each encompassing a range of challenging illumination and weather conditions: the driving dataset SELMA [42] and the FLYAWARE-S dataset introduced in this work. Both datasets are based on the CARLA simulator [8] for image generation, making them ideal choices for our research due to their shared framework. Then, our method is adapted in a federated fashion to real-world datasets: for cars we selected the ACDC dataset, supplemented by Cityscapes [7] for the clear samples as described in the Suppl. Mat. As the drone counterpart, we used our adverse-weather translated dataset FLYAWARE-R, which offers labeled frames captured from aerial views. Additionally, to enhance the robustness of our approach, we performed also tests using the VisDrone object detection dataset for clients’ training as training at client side is unsupervised. In this setting the entire FLYAWARE-R dataset can be used for testing purposes (*i.e.* XL) for more reliable results. The adverse translation of FLYAWARE-R is described in Sec. 5. All the extended datasets and splits are referenced in Fig. 3 and will be available at the link: [\[soon\]](#)

**Server pretraining.** We chose DeepLabV3 architecture with MobileNetV2 as in [37]. We trained our model on the source synthetic dataset using a decreasing power-law learning rate  $\eta$ , starting at  $\eta = 5e - 3$  with a power of 0.9. The optimization used SGD with momentum 0.9 and no weight decay, lasting for 5 epochs with batch size 16. For the weather classifier, we trained a 3-layer ConvNet with batch size 88, 8 epochs and SGD optimizer with learning rate  $1e - 4$ .

**Clients Adaptation.** For the target dataset, experiments were run with a fixed learning rate of  $\eta = 1e - 4$  with SGD optimizer. The training involved 5 clients per round for a total of  $R = 100$  rounds, with  $\lambda_{cl} = 140$ . The pseudo-label teacher model was updated at the end of each round. For the optimizer of the manifolds, we use RiemmanianAdam as in [40] with  $\gamma = 0.1$  as initialization, learning rate equal to  $1e - 3$  and weight decay of  $4e - 4$ .

## 7 Experimental Results

The results are detailed in Tab. 2, which reports the average mIoU for cars, drones and a combined score. The latter is computed using the average for the classes present in both datasets and the car mIoU otherwise. For comparison, we initially examined 3 supervised settings: 1) the source only approach, which relies exclusively on synthetic labeled data from the source domains for training; 2) the fully centralized approach, where all available data is used to train the network specifically on the target domain (250 epochs,  $lr = 5e - 3$ ); 3) the upper limit scenario for the federated model, where it undergoes fine-tuning with full supervision on the clients ( $R = 250$ ). In the unsupervised setting, (i.e., in the context of FFREEDA), we explore two strategies: the standard FedAvg [27] combined with our self-training approach, and the main competitor, LADD [37]. Notably, unlike our strategy, LADD conducts dataset stylization from the

**Table 3 and 4:** Motivation of our approach: viewpoints generalization (Tab. 3); generalization to different weather conditions (Tab. 4).

Pretrain on	Source Only	Adapted		Pretrain	Adapt	Clear	Night	Rain	Fog	All
		Separately	Jointly							
Car+Drone	22.70	28.95	28.96	Clear	-	23.43	6.43	24.93	25.50	18.28
Car only	18.23	25.17	25.24	All	-	25.41	13.62	26.72	26.08	22.69
Drone only	15.25	14.37	13.68	Clear	Clear	26.87	1.02	8.02	9.86	14.36
				Clear	All	25.97	7.87	25.70	23.16	18.11
				All	Clear	30.96	10.85	22.22	26.38	25.03
				All	All	<b>31.73</b>	<b>14.18</b>	<b>34.19</b>	<b>29.86</b>	<b>28.96</b>

target domain, assuming prior knowledge of the client data distribution during pretraining. We pretrain LADD on our synthetic adverse weather dataset to ensure comparability, maintaining the target’s average style as outlined in [37].

The large domain shift between the source and target domains is clear from the mIoU of 22.70% achieved by the source only training compared to 58.08% of the target training. Although the performance increases by almost 13% by fine-tuning the source only pretraining, assuming labeled data on the client side is not very realistic. In the unsupervised scenario, the baseline approach of using self-teaching with pseudo-labels together with FedAvg leads to a score of 26.10%, with a relatively small improvement from the source only proving that simple FL strategies struggle in this challenging setting. LADD [37] allows to improve performances to 26.96%, an improvement of around 1% compared to FedAvg. Our approach, in comparison to FedAvg and LADD, demonstrates a better improvement over the source only baseline reaching a mIoU of 28.96%. In particular notice how the gain is also well-distributed across car and drone agents, meaning that our strategy can effectively align with the intrinsic distribution shift that different viewpoints introduce. Notably, our approach is the only able to improve the source only results on both cars and drones, while competitors struggle with drone imagery since they are not able to generalize well

to both and trade-off the better performances on cars with a reduction of the accuracy on drones. Qualitative results are reported in the Suppl. Mat.

**Generalization capabilities of the proposed approach.** We perform further tests to evaluate the capability of our approach to adapt to different viewpoints and weather conditions. Specifically, in Tab. 3 we can underline the following: 1) Jointly pretraining on both car and drones improves the overall mIoU of 4.47% compared to car-only and 7.45% to drone-only; 2) Adapting to car and drones together leads to roughly the same performances of adapting separately two models (one for cars and one for drones), i.e., the model generalize well across the two agents even when only one viewpoint is provided; 3) In the drone-only setting, the limited number of clients results in poor generalization and overconfidence in predictions. In Tab. 4, we underline that: 1) When pre-training with synthetic data from all weather conditions the model improves on all, especially the night; moreover, adapting from clear weather only results in poor generalization when adapting to real data; 2) Although adapting with only clear weather data increases the mIoU on clear weather itself, it worsens the performance on almost all the other conditions.

**Table 5:** Ablation of the proposed method components.

$\mathcal{L}_{st}$	AG	$\mathcal{L}_{cl}$	BN	Car	Drone	All
				19.96	33.11	22.70
✓				25.00	30.25	26.10
✓	✓			24.75	33.49	26.57
✓	✓		✓	24.91	34.55	26.92
✓	✓	✓		27.17	33.60	28.51
✓	✓	✓	✓	<b>27.45</b>	<b>34.69</b>	<b>28.96</b>

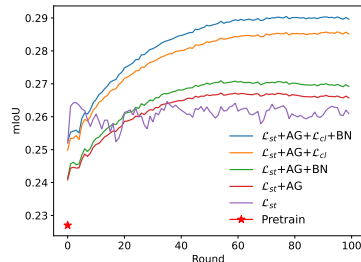


**Fig. 4:** Training curves of the ablation.

**Ablation studies.** Tab. 5 shows an extensive ablation of the various modules of the proposed approach together and Fig. 4 the corresponding training curves. The aggregation strategy of Eq. (12) stabilizes the self-training and avoids performance decrease on unbalanced clients (*i.e.* drones). The batch normalization effect is visible in cars and drones (+3.4% overall). Observe that the testing set of drones is more balanced in terms of weather categories ( $\frac{1}{4}$  each), making it more noticeable. The hyperbolic prototypes allow for improving the generalization of the feature spaces compared to the baseline, achieving 28.51%. In Suppl. Mat. a comprehensive examination of the advantages over the standard Euclidean space is provided. Finally, adding each component leads to the final score of 28.96%. Overall, the contributions of all the components jointly produce a gain of over 6.26% of mIoU on the source only. Further ablation on the hyperparameters is in the Suppl. Mat.

## 8 Conclusion

In this paper we introduced a new federated learning scenario, addressing the challenges of heterogeneous autonomous agents in adverse weather conditions. The contributions include a realistic federated setting where clients are unsupervised and a versatile model seamlessly integrating aerial views. To achieve these results, we introduced the FLYAWARE dataset for semantic segmentation in adverse weather. The proposed method, HyperFLAW, employs weather-aware batch normalization layers to mitigate domain shifts across diverse weather conditions. Additionally, it leverages prototype-based learning in the hyperbolic space, contributing a novel method for consistent training in this challenging federated setting. By extending the scope to different types of vehicles and addressing real-world challenges such as adverse weather and privacy preservation, our contributions lay a foundation for future advancements in autonomous driving. Further research will be devoted to the exploitation of multi-modal data and to more advanced ad-hoc adaptation strategies for adverse weather conditions.

### Acknowledgment

This work was supported in part by the European Union through the Italian National Recovery and Resilience Plan (NRRP) of NextGenerationEU, a partnership on “Telecommunications of the Future” (Program “RESTART”) under Grant PE0000001.

### References

1. Araslanov, N., Roth, S.: Self-supervised augmentation consistency for adapting semantic segmentation. In: Proceedings of the IEEE/CVF Conference on Computer Vision and Pattern Recognition. pp. 15384–15394 (2021) [3](#)
2. Atigh, M.G., Schoep, J., Acar, E., Van Noord, N., Mettes, P.: Hyperbolic image segmentation. In: Proceedings of the IEEE/CVF conference on computer vision and pattern recognition. pp. 4453–4462 (2022) [4](#)
3. Brüggemann, D., Sakaridis, C., Truong, P., Van Gool, L.: Refign: Align and refine for adaptation of semantic segmentation to adverse conditions. In: Proceedings of the IEEE/CVF Winter Conference on Applications of Computer Vision. pp. 3174–3184 (2023) [3](#)
4. Caldarola, D., Caputo, B., Ciccone, M.: Window-based model averaging improves generalization in heterogeneous federated learning. In: Proceedings of the IEEE/CVF International Conference on Computer Vision. pp. 2263–2271 (2023) [9](#)
5. Chellapandi, V.P., Yuan, L., Brinton, C.G., Žak, S.H., Wang, Z.: Federated learning for connected and automated vehicles: A survey of existing approaches and challenges. *IEEE Transactions on Intelligent Vehicles* (2023) [3](#), [4](#)
6. Choi, J., Kim, T., Kim, C.: Self-ensembling with gan-based data augmentation for domain adaptation in semantic segmentation. In: Proceedings of the IEEE/CVF International Conference on Computer Vision. pp. 6830–6840 (2019) [3](#)

7. Cordts, M., Omran, M., Ramos, S., Rehfeld, T., Enzweiler, M., Benenson, R., Franke, U., Roth, S., Schiele, B.: The cityscapes dataset for semantic urban scene understanding. In: Proceedings of the IEEE conference on computer vision and pattern recognition. pp. 3213–3223 (2016) [12](#), [20](#)
8. Dosovitskiy, A., Ros, G., Codevilla, F., Lopez, A., Koltun, V.: Carla: An open urban driving simulator. In: Conference on robot learning. pp. 1–16. PMLR (2017) [10](#), [12](#)
9. Du, D., Qi, Y., Yu, H., Yang, Y., Duan, K., Li, G., Zhang, W., Huang, Q., Tian, Q.: The unmanned aerial vehicle benchmark: Object detection and tracking. In: Proceedings of the European conference on computer vision (ECCV). pp. 370–386 (2018) [11](#)
10. Eftekhari, A., Sax, A., Malik, J., Zamir, A.: Omnidata: A scalable pipeline for making multi-task mid-level vision datasets from 3d scans. In: Proceedings of the IEEE/CVF International Conference on Computer Vision. pp. 10786–10796 (2021) [11](#)
11. Fantauzzo, L., Fani, E., Caldarola, D., Tavera, A., Cermelli, F., Ciccone, M., Caputo, B.: Feddrive: Generalizing federated learning to semantic segmentation in autonomous driving. In: 2022 IEEE/RSJ International Conference on Intelligent Robots and Systems (IROS). pp. 11504–11511. IEEE (2022) [3](#)
12. Gao, Z., Wu, Y., Jia, Y., Harandi, M.: Curvature generation in curved spaces for few-shot learning. In: Proceedings of the IEEE/CVF international conference on computer vision. pp. 8691–8700 (2021) [3](#)
13. Gasperini, S., Morbitzer, N., Jung, H., Navab, N., Tombari, F.: Robust monocular depth estimation under challenging conditions. In: Proceedings of the IEEE/CVF international conference on computer vision. pp. 8177–8186 (2023) [11](#)
14. Guo, Y., Wang, X., Chen, Y., Yu, S.X.: Clipped hyperbolic classifiers are super-hyperbolic classifiers. In: Proceedings of the IEEE/CVF Conference on Computer Vision and Pattern Recognition. pp. 11–20 (2022) [3](#)
15. Hoyer, L., Dai, D., Van Gool, L.: Daformer: Improving network architectures and training strategies for domain-adaptive semantic segmentation. In: Proceedings of the IEEE/CVF Conference on Computer Vision and Pattern Recognition. pp. 9924–9935 (2022) [3](#)
16. Hu, X., Fu, C.W., Zhu, L., Heng, P.A.: Depth-attentional features for single-image rain removal. In: Proceedings of the IEEE/CVF Conference on computer vision and pattern recognition. pp. 8022–8031 (2019) [11](#)
17. Khrukov, V., Mirvakhabova, L., Ustinova, E., Oseledets, I., Lempitsky, V.: Hyperbolic image embeddings. In: Proceedings of the IEEE/CVF Conference on Computer Vision and Pattern Recognition. pp. 6418–6428 (2020) [3](#)
18. Klinghoffer, T., Phillion, J., Chen, W., Litany, O., Gojcic, Z., Joo, J., Raskar, R., Fidler, S., Alvarez, J.M.: Towards viewpoint robustness in bird’s eye view segmentation. In: Proceedings of the IEEE/CVF International Conference on Computer Vision. pp. 8515–8524 (2023) [2](#)
19. Li, J., Yu, Z., Du, Z., Zhu, L., Shen, H.T.: A comprehensive survey on source-free domain adaptation. *IEEE Transactions on Pattern Analysis and Machine Intelligence* (2024) [3](#)
20. Li, Q., He, B., Song, D.: Model-contrastive federated learning. In: Proceedings of the IEEE/CVF conference on computer vision and pattern recognition. pp. 10713–10722 (2021) [3](#)
21. Li, T., Sahu, A.K., Zaheer, M., Sanjabi, M., Talwalkar, A., Smith, V.: Federated optimization in heterogeneous networks. *Proceedings of Machine learning and systems* **2**, 429–450 (2020) [3](#)



22. Li, X., Jiang, M., Zhang, X., Kamp, M., Dou, Q.: Fedbn: Federated learning on non-iid features via local batch normalization. arXiv preprint arXiv:2102.07623 (2021) [7](#)
23. Liu, Y., Deng, J., Gao, X., Li, W., Duan, L.: Bapa-net: Boundary adaptation and prototype alignment for cross-domain semantic segmentation. In: Proceedings of the IEEE/CVF international conference on computer vision. pp. 8801–8811 (2021) [3](#)
24. Luo, Y., Zheng, L., Guan, T., Yu, J., Yang, Y.: Taking a closer look at domain shift: Category-level adversaries for semantics consistent domain adaptation. In: Proceedings of the IEEE/CVF conference on computer vision and pattern recognition. pp. 2507–2516 (2019) [3](#)
25. Lyu, Y., Vosselman, G., Xia, G.S., Yilmaz, A., Yang, M.Y.: Uavid: A semantic segmentation dataset for uav imagery. ISPRS journal of photogrammetry and remote sensing **165**, 108–119 (2020) [11](#), [22](#)
26. Ma, R., Fang, P., Drummond, T., Harandi, M.: Adaptive poincaré point to set distance for few-shot classification. In: Proceedings of the AAAI conference on artificial intelligence. vol. 36, pp. 1926–1934 (2022) [3](#)
27. McMahan, B., Moore, E., Ramage, D., Hampson, S., y Arcas, B.A.: Communication-efficient learning of deep networks from decentralized data. In: Artificial Intelligence and Statistics (AISTATS). pp. 1273–1282. PMLR (2017) [3](#), [9](#), [12](#), [13](#), [25](#)
28. Mei, K., Zhu, C., Zou, J., Zhang, S.: Instance adaptive self-training for unsupervised domain adaptation. In: Computer Vision–ECCV 2020: 16th European Conference, Glasgow, UK, August 23–28, 2020, Proceedings, Part XXVI 16. pp. 415–430. Springer (2020) [3](#)
29. Mettes, P., Atigh, M.G., Keller-Ressel, M., Gu, J., Yeung, S.: Hyperbolic deep learning in computer vision: A survey. arXiv preprint arXiv:2305.06611 (2023) [3](#), [8](#)
30. Michieli, U., Basetton, M., Agresti, G., Zanuttigh, P.: Adversarial learning and self-teaching techniques for domain adaptation in semantic segmentation. IEEE Transactions on Intelligent Vehicles **5**(3), 508–518 (2020) [3](#)
31. Ren, H., Yang, Y., Wang, H., Shen, B., Fan, Q., Zheng, Y., Liu, C.K., Guibas, L.J.: Adela: Automatic dense labeling with attention for viewpoint shift in semantic segmentation. In: Proceedings of the IEEE/CVF Conference on Computer Vision and Pattern Recognition. pp. 8079–8089 (2022) [2](#)
32. Rizzoli, G., Barbato, F., Caligiuri, M., Zanuttigh, P.: Syndrone-multi-modal uav dataset for urban scenarios. In: Proceedings of the IEEE/CVF International Conference on Computer Vision. pp. 2210–2220 (2023) [10](#), [25](#)
33. Saito, K., Watanabe, K., Ushiku, Y., Harada, T.: Maximum classifier discrepancy for unsupervised domain adaptation. In: Proceedings of the IEEE conference on computer vision and pattern recognition. pp. 3723–3732 (2018) [3](#)
34. Sakaridis, C., Dai, D., Van Gool, L.: Acdc: The adverse conditions dataset with correspondences for semantic driving scene understanding. In: Proceedings of the IEEE/CVF International Conference on Computer Vision. pp. 10765–10775 (2021) [10](#), [11](#), [20](#)
35. Sarlin, P.E., Trulls, E., Pollefeys, M., Hosang, J., Lynen, S.: Snap: Self-supervised neural maps for visual positioning and semantic understanding. Advances in Neural Information Processing Systems **36** (2024) [2](#)
36. Schwonberg, M., Niemeijer, J., Termöhlen, J.A., Schäfer, J.P., Schmidt, N.M., Gottschalk, H., Fingscheidt, T.: Survey on unsupervised domain adaptation for semantic segmentation for visual perception in automated driving (2023) [3](#)

37. Shenaj, D., Fani, E., Toldo, M., Caldarola, D., Tavera, A., Michieli, U., Ciccone, M., Zanuttigh, P., Caputo, B.: Learning across domains and devices: Style-driven source-free domain adaptation in clustered federated learning. In: Proceedings of the IEEE/CVF Winter Conference on Applications of Computer Vision. pp. 444–454 (2023) [2](#), [3](#), [4](#), [5](#), [6](#), [9](#), [11](#), [12](#), [13](#), [25](#)
38. Shenaj, D., Rizzoli, G., Zanuttigh, P.: Federated learning in computer vision. *IEEE Access* (2023) [3](#)
39. Shenaj, D., Toldo, M., Rigon, A., Zanuttigh, P.: Asynchronous federated continual learning. In: Proceedings of the IEEE/CVF Conference on Computer Vision and Pattern Recognition. pp. 5054–5062 (2023) [9](#)
40. van Spengler, M., Berkhout, E., Mettes, P.: Poincare resnet. In: Proceedings of the IEEE/CVF International Conference on Computer Vision. pp. 5419–5428 (October 2023) [8](#), [12](#)
41. van Spengler, M., Wirth, P., Mettes, P.: Hypll: The hyperbolic learning library. arXiv preprint arXiv:2306.06154 (2023) [8](#)
42. Testolina, P., Barbato, F., Michieli, U., Giordani, M., Zanuttigh, P., Zorzi, M.: Selma: Semantic large-scale multimodal acquisitions in variable weather, daytime and viewpoints. *IEEE Transactions on Intelligent Transportation Systems* (2023) [10](#), [12](#), [20](#)
43. Toldo, M., Maracani, A., Michieli, U., Zanuttigh, P.: Unsupervised domain adaptation in semantic segmentation: a review. *Technologies* **8**(2), 35 (2020) [3](#)
44. Tsai, Y.H., Hung, W.C., Schulter, S., Sohn, K., Yang, M.H., Chandraker, M.: Learning to adapt structured output space for semantic segmentation. In: Proceedings of the IEEE conference on computer vision and pattern recognition. pp. 7472–7481 (2018) [3](#)
45. Tzeng, E., Hoffman, J., Zhang, N., Saenko, K., Darrell, T.: Deep domain confusion: Maximizing for domain invariance. arXiv preprint arXiv:1412.3474 (2014) [3](#)
46. Xia, R., Zhao, C., Zheng, M., Wu, Z., Sun, Q., Tang, Y.: Cmda: Cross-modality domain adaptation for nighttime semantic segmentation. In: Proceedings of the IEEE/CVF International Conference on Computer Vision. pp. 21572–21581 (2023) [3](#)
47. Yang, Y., Soatto, S.: Fda: Fourier domain adaptation for semantic segmentation. In: Proceedings of the IEEE/CVF conference on computer vision and pattern recognition. pp. 4085–4095 (2020) [3](#)
48. Yu, F., Chen, H., Wang, X., Xian, W., Chen, Y., Liu, F., Madhavan, V., Darrell, T.: Bdd100k: A diverse driving dataset for heterogeneous multitask learning. In: Proceedings of the IEEE/CVF conference on computer vision and pattern recognition. pp. 2636–2645 (2020) [11](#)
49. Zhang, N., Zhang, L., Cheng, Z.: Towards simulating foggy and hazy images and evaluating their authenticity. In: International Conference on Neural Information Processing. pp. 405–415. Springer (2017) [11](#)
50. Zhang, P., Zhang, B., Zhang, T., Chen, D., Wang, Y., Wen, F.: Prototypical pseudo label denoising and target structure learning for domain adaptive semantic segmentation. In: Proceedings of the IEEE/CVF conference on computer vision and pattern recognition. pp. 12414–12424 (2021) [3](#)
51. Zhang, Q., Zhang, J., Liu, W., Tao, D.: Category anchor-guided unsupervised domain adaptation for semantic segmentation. *Advances in neural information processing systems* **32** (2019) [3](#)
52. Zheng, Z., Wu, Y., Han, X., Shi, J.: Forkgan: Seeing into the rainy night. In: Computer Vision–ECCV 2020: 16th European Conference, Glasgow, UK, August 23–28, 2020, Proceedings, Part III 16. pp. 155–170. Springer (2020) [11](#)

53. Zhu, P., Wen, L., Du, D., Bian, X., Fan, H., Hu, Q., Ling, H.: Detection and tracking meet drones challenge. *IEEE Transactions on Pattern Analysis and Machine Intelligence* **44**(11), 7380–7399 (2021) [11](#), [22](#)
54. Zou, Y., Yu, Z., Kumar, B., Wang, J.: Unsupervised domain adaptation for semantic segmentation via class-balanced self-training. In: *Proceedings of the European conference on computer vision (ECCV)*. pp. 289–305 (2018) [3](#)

# When Cars meet Drones: Hyperbolic Federated Learning for Source-Free Domain Adaptation in Adverse Weather

## *Supplementary Material*

Giulia Rizzoli\*<sup>id</sup>, Matteo Caligiuri\*<sup>id</sup>, Donald Shenaj<sup>id</sup>, Francesco Barbato<sup>id</sup>,  
and Pietro Zanuttigh <sup>id</sup>

University of Padova, Italy  
firstname.lastname@dei.unipd.it

This document contains the supplementary material for the paper *When Cars meet Drones: Hyperbolic Federated Learning for Source-Free Domain Adaptation in Adverse Weather*. We start by introducing additional details on the employed datasets. We then proceed with ablations supporting the usage of the weather batch-normalization and of hyperbolic prototypes. Finally, we show further experimental data including per-class accuracy scores and qualitative results.

## S1 Data Selection and Distribution

In the main paper, we introduced the **FLYAWARE** aerial dataset since it is a novel contribution. Conversely, we offered fewer details for car driving datasets, as we relied on existing datasets. Here we will first describe the technical choices adopted to enable distributed learning on car agents in adverse weather. Then, some additional details on weather distribution among clients are provided.

### S1.1 Driving Datasets

For the synthetic source dataset for cars, we used the **SELMA** dataset [42]. It offers a comprehensive set of 27 weather and daytime conditions, resulting in a vast dataset of over 20M samples. To better align with the weather scenarios considered in real data [34], we opted not to use the standard SELMA split, but downloaded over 24k samples in the *ClearNoon*, *ClearNight*, *HardRainNoon*, *MidFoggyNoon* splits. In total, for this work, we employed almost 100k SELMA samples from the Desk Cam point of view that match the one used in the real-world dataset. As the real counterpart, we used the **ACDC** dataset, from which we selected the 3 domains — night, rain, and fog — that match our pretraining. As ACDC lacks images in clear weather, we supplemented it with daytime images coming from the Cityscapes dataset [7], which is the most similar to ACDC. Note that, the ACDC dataset has been built to create an adverse condition version of Cityscapes, and shares the same class-set. Cityscapes provides more samples than those in the thematic splits by ACDC. Therefore, we subsampled its training set to match the sizes. Since the goal was to select clear weather conditions, we

---

\* These authors contributed equally to this work.

devised an automatic way of assigning a sunlit level (Eq. S1) to each image and selected the needed images by sorting them according to this metric:

$$\text{sunlit}(\mathbf{X}) = \sum_{c \in \{r, g, b\}} \frac{1}{HW} \sum_{i=0}^W \sum_{j=0}^W \mathbf{X}[i, j, c] \quad (\text{S1})$$

As shown in Tab. 1 in the main paper, we selected a set of images to match the total count of all other conditions combined, aiming for a ratio of three clear sky images to one adverse condition. This decision was driven by the desire to retain “clear sky” as the most probable scenario in real-world contexts. In Fig. S1 we report some examples of samples with their rating (a bright one, a dark one and a mid-range one).

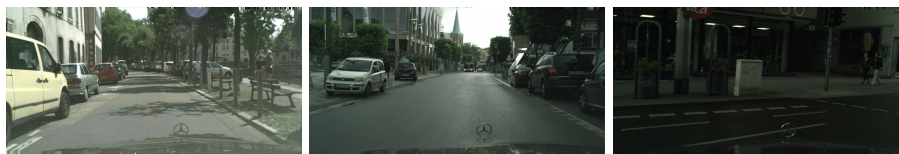


**Fig. S1:** Cityscapes samples and corresponding *sunlit* score. Decreasing from the left, high/mid/low-score ( $\sim 300/200/100$ ).

### S1.2 Weather Heterogeneity

Fig. S2 illustrates the weather distribution among clients in the configuration **ACDC+FLYAWARE-R**. We deliberately supplied clear day samples to each client to emulate a common scenario where clear daylight conditions prevail, with fewer instances of challenging weather conditions. This introduces an inherent challenge as adverse weather data samples are less prevalent. Additionally, the imbalance among clients further complicates the scenario. Fig. S3 shows the weather distribution for clients in the **ACDC+FLYAWARE-R-XL** setup. While this configuration exhibits better data balance across clients, it introduces

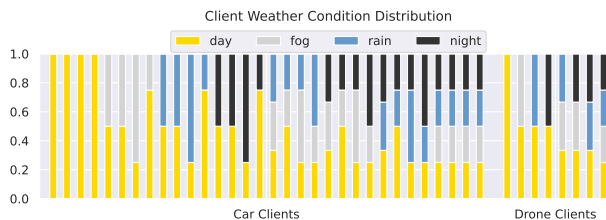


**Fig. S2:** Distribution of weather conditions across clients (ACDC and FLYAWARE-R).

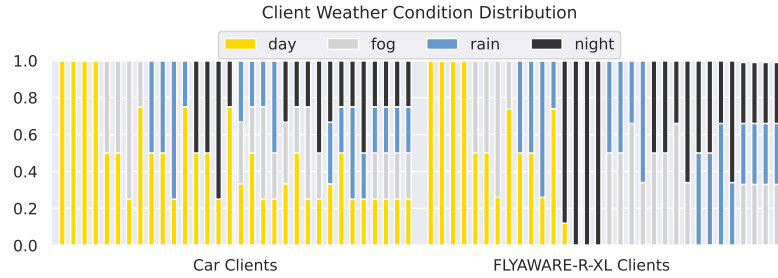


**Fig. S3:** Distribution of weather conditions across clients (ACDC and FLYAWARE-R-XL).

new complexities: some drone clients exclusively operate in adverse conditions, and the training and testing domains originate from different datasets (VisDrone [53] and UAVid [25], respectively). Notably, VisDrone images offer real night data, whereas we utilized domain-translated images for fog and rain using the same strategies described in the main paper.

## S2 Impact of Weather-Batch Normalization

As shown in Tab. 5 of the main paper, the inclusion of ad-hoc batch norms (BNs) enhances performance in comparison to utilizing a non-personalized network. First of all, in Fig. S4, we show in detail the architecture of the weather classifier. Although the classifier model is simple, it achieves an accuracy of 98.96% on the source synthetic datasets used to train it and of 72.37% on the real world target ones.

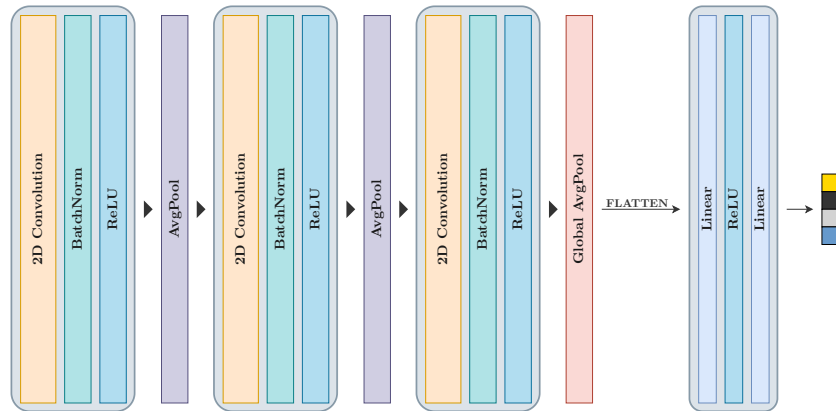


**Fig. S4:** Weather classifier architecture model.

**Table S1:** Effect of the different modules on the weather.

Modules	Clear	Night	Rain	Fog
Pretrain	25.41	13.62	26.72	26.08
ST + AG w/o BN	29.27	13.47	29.47	27.86
ST + AG w BN	26.81	13.50	30.19	28.86
ALL w/o BN	31.58	14.04	30.53	28.93
ALL w BN	31.73	14.18	34.19	29.86

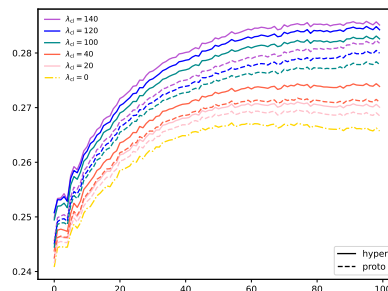
We further examine in Tab. S1 the advantage of adapting the system to accommodate different weather conditions as a remarkable feature for the decision-making of autonomous driving agents. The basic self-training strategy, coupled with the proposed server-side aggregation scheme, has shown stability and an overall improvement over pretraining. However, due to the prevalence of clear-day images in most clients’ samples, the network tends to learn more about this weather condition. Introducing the personalized weather BNs helps to mitigate this, improving performances in adverse weather conditions, with an mIoU increase of 3% on Rain and 1.78% on Fog. Similar results are evident when comparing the full method with and without the weather BNs, showcasing mIoU increases of 3.66% on Rain and 0.93% on Fog. As a side note, the most difficult scenario remains the night where the improvement over the pretraining is just 0.56% of mIoU. Overall, we remark on the significance of incorporating personalized weather BNs for mitigating bias towards clear day images and enhancing performance across various weather conditions.

As a final note, considering that modern vehicles often have access to real-time weather information through several sensors (e.g., automatic windshield wipers for rain detection, clock or optical light detection for night and fog), and the weather information might be directly obtained.

### S3 Analysis of class prototypes effectiveness

#### Hyperbolic vs. Euclidean Prototypes

In Fig. S5, we show the training curves for both Euclidean prototypes and hyperbolic ones employing different values of the weighting parameter for the prototype loss  $\lambda_{cl}$ . Notably, hyperbolic space prototypes consistently allow for an increase in performances across different  $\lambda_{cl}$  values. The key strength of the hyperbolic space lies in its ability to effectively represent distances between feature vectors, a crucial factor in tasks like clustering where having a distance function capturing meaningful relationships among data points is essential.

**Fig. S5:** Euclidean vs hyperbolic prototypes.

**Setting of the  $\lambda_{cl}$  parameter** Fig. S6 shows the mIoU for different values of the  $\lambda_{cl}$  parameter. Best performances are achieved in the range 140-180, with a quite stable maxima.

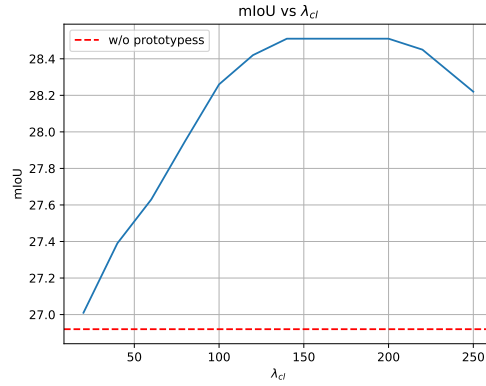


**Fig. S6:** Tuning on  $\lambda_{cl}$  weight.

## S4 Per-class Results

Tab. S2 contains a more detailed version of the results in Tab. 5 of the main paper that shows also the class-by-class accuracy. As common on the employed datasets, the mIoU is higher in the common classes (e.g., road or building) and lower in the rare and more challenging ones. However, it can be seen that by adding the various components of the model, results tend to increase consistently in most classes, even if a few challenging ones remain hard to detect. Some classes like traffic sign, car or bicycle show impressive improvements. On the other side, there are a few cases in which our approach does not improve the results on some under-represented classes such as terrain and rider.

**Table S2:** Per class IoU for the proposed approach and its ablated versions.

ST	AG	CL	BN	road	sidewalk	building	wall	fence	pole	traffic light	traffic sign	vegetation	terrain	sky	person	rider	car	truck	bus	train	motorcycle	bicycle	All
				35.4	5.7	55.8	4.6	4.2	14.2	13.3	10.9	61.9	6.3	43.7	26.0	17.2	11.1	3.3	3.8	1.4	8.9	10.7	22.7
✓				43.7	22.0	57.2	6.6	4.7	15.8	9.8	13.9	50.2	5.7	68.4	24.3	11.4	34.6	8.9	4.7	3.5	16.0	14.9	26.1
✓	✓			43.9	23.2	59.2	7.1	5.9	16.2	11.1	14.8	55.3	6.1	58.5	26.0	11.9	34.2	9.2	4.3	3.0	15.8	13.5	26.6
✓	✓	✓		43.8	23.6	59.7	6.9	5.9	15.9	10.7	14.8	56.5	5.1	60.6	25.4	11.9	37.7	9.0	4.5	2.8	15.1	13.0	26.9
✓	✓	✓	✓	46.8	22.4	59.9	7.4	6.7	17.6	17.0	22.4	56.6	7.1	62.6	25.4	10.5	35.5	9.5	6.9	3.7	16.6	25.7	28.5
✓	✓	✓	✓	47.2	22.7	60.6	7.0	6.7	17.3	16.8	22.7	57.7	5.9	64.9	25.4	10.6	36.9	9.3	6.8	3.5	16.8	25.5	29.0



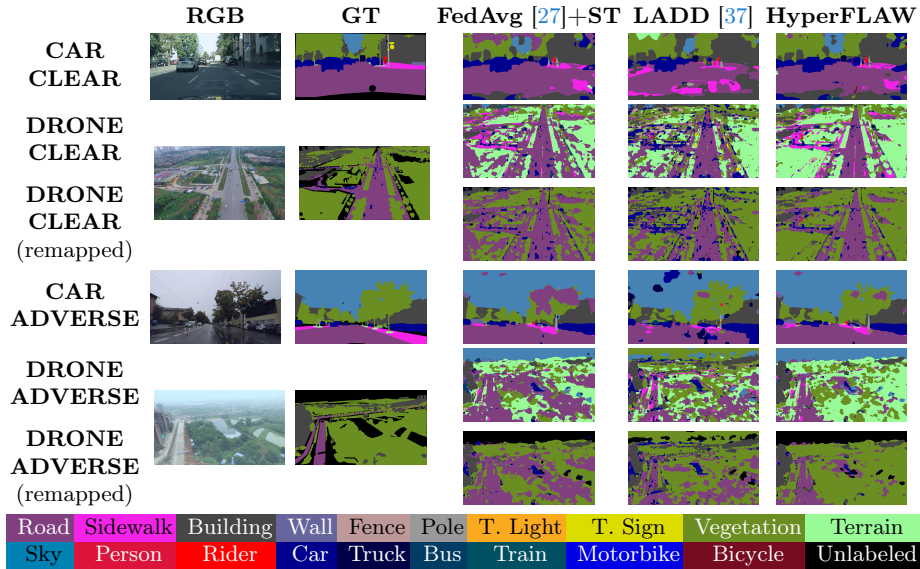


Fig. S7: Qualitative results.

## S5 Qualitative Results

Fig. S7 shows some qualitative results for car and drone samples in both clear and adverse weather. FedAvg [27] and LADD [37] appear to be overconfident on the road and car classes, respectively. While our model adeptly captures the structure of the street better than other models in both adverse and non-adverse conditions, the adverse conditions images remain a challenging aspect. For drones, the discrepancies between the predicted classes and the ground truth arise also due to the fact that the network is trained on a superset of classes beyond those present in the drone dataset. Notice that sometimes the network assigns “fine” classes that share a semantic affiliation with the respective “coarse” classes, e.g., predict terrain instead of vegetation, but on the drone dataset labeling terrain is not present and terrain samples have ground truth set to vegetation. The same thing happens for the sidewalk and road or rider and person. For this reason, we remapped the 19 classes of the full set into the 5 drone ones using the mapping proposed in [32]. The figure shows both the original prediction maps from the network and the ones obtained after remapping the 19 classes into the 5 of the drone datasets. The comparison with the ground truth shows that some predictions not matching are just due to the different types of labeling in drone and car datasets.